The low-crystallinity PVDF/PMMA/PEG/TiO₂ Type Polymer Diaphragm Prepared by Phase Inversion Method

Hong Gao, Mingpeng Mu, Zhongcai Shao,

School of Environment and Chemical Engineering, Shenyang Ligong University
*E-mail: 1641796109@qq.com

In order to improve the lithium ion battery of Poly-Vinylidene Fluoride (PVDF) conductivity and decrease crystallization of PVDF based polymer separator, introducing Poly-Methyl-Methacrylate (PMMA) and Poly-Vinylidene Fluoride (PVDF) to blend and doping organic additives PEG and inorganic nanomaterials TiO_2. The PVDF/PMMA/PEG/TiO₂ typed polymer diaphragm was prepared by Phase inversion method. Through the analysis of the porosity, ionic conductivity, charging and discharging to test, micro-morphology and electrochemical properties of the prepared PVDF/PMMA/PEG/TiO₂ porous separators, the optimum technological conditions for the preparation of the separator is polymer concentration of 8%, PMMA of 30% and PEG of 30%; the content of nanometer TiO_2 is 5%; the content of C_2H_5OH is 3%; the reaction temperature is 45°C, and the temperature is 30%. Under the best scheme, the crystallinity of the prepared polymer diaphragm is lower than that of the pure PVDF diaphragm. The porosity of the polymer diaphragm is 81.5%. The ionic conductivity is 5.2mS/cm, the tensile strength is 1183kg/cm². The electrochemical stability window is 4.68v, which is higher than 4.5v. It can meet the normal working requirements of lithium-ion batteries.

1. INTRODUCTION

At present, the materials used for preparing the lithium ion battery separator are mainly thermoplastic polyolefin materials, such as PE, PP, and most of the diaphragm is composite structure (PP / PE / PP) [1]. It is higher strength and better chemical stability. It has the function of automatic shrinkage hole, which can prevent explosion caused by overheating at the condition of higher than the glass transition temperature (170°C). It is a relatively reliable lithium-ion battery separator material [2]. The polyolefin diaphragm has the small polarity and the high degree of crystalline, but the electrolyte of lithium ion batteries is high polar organic solvent, resulting in relatively poor separator and

electrolyte affinity. Almost no swelling of the electrolyte, and the diaphragm to the electrolyte liquid absorption rate is low [3]. This can result in high resistance and poor cycling performance [4]. At the same time, the polyolefin separator resistance to chemical corrosion is not high and easy to aging, and it could be damaged and cause explosions in shortcircuiting [5]. These factors affect the lithium-ion battery cycle life and high-power discharge safety.

The separator materials of lithium-ion batteries of good chemical electrochemical stability and good affinity to electrolyte are widely concerned and studied [6-8]. The modification methods of PVDF separator mainly include irradiation modification [9], electrostatic spinning, plasma modification, blending modification, chemical modification and so on [10-15]. Surface modifications by irradiation treatment obviously improve the ionic conductivity performance of the separators, but the thermal stability and mechanical property still require improvement [4]. Alternatively, the electrostatic spinning composite fiber separators show excellent thermal stability and cycling performance, but the preparation process is cumbersome, time consuming and too expensive for manufacturing. But the blending modification is the most convenient and effective method for the modification of PVDF separator [16-20]. In this paper, the PVDF polymer diaphragm was modified by the method of Poly-Methyl-Methacrylate (PMMA) blending, doping organic plasticizer PEG and nanometer TiO_2 to further improve the electrochemical performance of the polymer diaphragm.

2. EXPERIMENT

2.1. Principle and procedure of experiment

The process of making separator by phase inversion can be divided into dry method and wet process according to different process. Both dry and wet methods firstly configure the polymer matrix solution and then phase separation of a three-dimensional network structure by physical means [21-22]. In this paper, the dry process is first used, followed by a wet process to prepare a polymer diaphragm. In the preparation of porous separator Phase inversion method, the additive PEG can affect the solubility of the solvent, changing the dissolved state of polymer separator liquid, and it can improve the mass transfer of non-solvents in liquid separators, accelerate the rate of gel precipitation, and cause instantaneous phase separation. Therefore, it contributes to pore formation of diaphragm formation, and it is not easily eluted during the late diaphragm formation process, thereby increasing the affinity with the separator to the electrolyte.

The polymer separator prepared was divided into two steps in this experiment. First, a polymer porous separator was prepared, and then it was immersed in an electrolyte and activated to become a polymer electrolyte separator. The specific experimental process is shown in Figure 1.
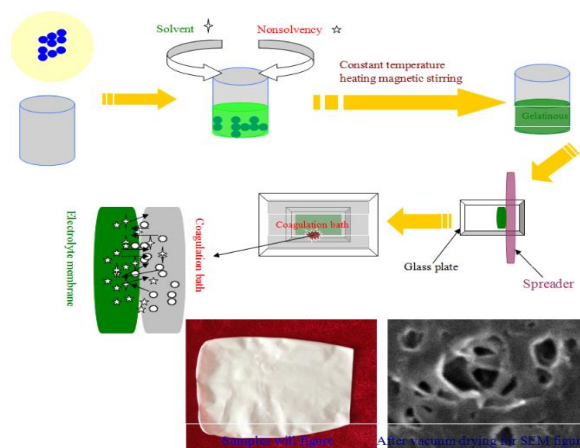
Figure 1. Flow chart of the experiment

The raw materials for this experiment include Poly-Vinylidene Fluoride (PVDF), Poly-Methyl-Methacrylate (PMMA), polyethylene glycol (PEG), nano-TiO_2, acetone and anhydrous ethanol. Select the percentage of polymer in the solvent, the mass percentage of the two polymers, the content of TiO_2, the amount of the non-solvent, and the reaction temperature were selected as the examination factors, and the porosity and the ionic conductivity were selected as indexes.

This experiment used the best process conditions of the previous PVDF/PMMA/PEG polymer separator [23], polymer concentration of 8%, Poly-Vinylidene Fluoride (PVDF) and Poly-Methyl-Methacrylate (PMMA) mass ratio is 7:3; the dosage of PEG was 30%; the dosage of C_2H_5OH was 3%, the reaction temperature is 45℃. Under these experimental parameters, nano-TiO_2 with 2%, 5%, 8% and 10% was added to study its influence on the properties of the polymers.

The interaction between various factors is not considered. The orthogonal experimental design is shown in Table 1 and 2.

Table 1. Factor level table

level	A Polymer percentage	B PVDF:PMMA	C TiO$_2$ percentage	D Non-solvent percentage	E temperature /°C
1	3%	7.2：2.8	2%	0%	45
2	5%	7.7：2.3	5%	1%	50
3	7%	8.2：1.8	8%	2%	55
4	9%	8.7：1.2	10%	3%	60

The concrete experiment steps are as follows: the PVDF and PMMA powders are mixed in a certain proportion of the container, by adding acetone, PEG, nanometer TiO_2 (average size 30nm) and anhydrous ethanol. After being ultrasonically shaken for 20min, put it in a water bath of a certain temperature and stir until it is gelatinous, static for a moment, coated diaphragm after 40-60s the separator together with the mold into the coagulation bath immersed in 24h, remove the separator

vacuum 80°C drying 12h.The porous separator is activated by 2h in the electrolyte to prepare the polymer diaphragm.

Table 2. Orthogonal experiment table

experiment	A	B	C	D	E	porosity	conductivity
1	1	1	1	1	1	---	---
2	1	2	2	2	2	---	---
3	1	3	3	3	3	---	---
4	1	4	4	4	4	---	---
5	2	1	2	3	4	---	---
6	2	2	1	4	3	---	---
7	2	3	4	1	2	---	---
8	2	4	3	2	1	---	---
9	3	1	3	4	2	---	---
10	3	2	4	3	1	---	---
11	3	3	1	2	4	---	---
12	3	4	2	1	3	---	---
13	4	1	4	2	3	---	---
14	4	2	3	1	4	---	---
15	4	3	2	4	1	---	---
16	4	4	1	3	2	---	---

2.2. Performance research methods

2.2.1 Research methods of Porosity

Porosity is the ratio of pore volume to total diaphragm volume, and porosity affects ionic conductivity, which is related to the interfacial stability of positive and negative electrode materials. The porosity of the polymer diaphragm is calculated by the method of liquid-absorbent calculation, which is used to soak the diaphragm in a known solvent and to calculate the pore volume occupied by the liquid by measuring the mass difference before and after the infiltration of the diaphragm. The complete dry-state polymer diaphragm is cut into a circular slice of the same diameter, and 5 samples are selected to be called the dry weight W_0. Then a certain mass of polymer separator is immersed in electrolyte (1.0 M $LiPF_6$/DEC+DMC (volume ratio 1:1)), and take out after two hours. Use a filter paper to dry the surface electrolyte, the weight was W_t, and the whole operation were carried out in the glove box [24-26]. The liquid absorption rate is calculated by the following formula:

$$\rho = (W_t - W_0)/W_0 \times 100\%$$

In the formula, W_t is the mass after absorbing electrolyte (g), W_0 is the mass before absorption of electrolyte (g).

2.2.2 Research methods of ionic conductivity

The ionic conductivity of polymer diaphragm is measured by the electrochemical impedance spectroscopy method, and the activated polymer diaphragm is placed between two smooth stainless

steel poles, and the analog battery are assembled. The polymer diaphragm area is slightly larger than the stainless steel plate, so as to avoid the short circuit of two electrode steel plates when assembling the battery. Use of the United States 2273 electrochemical workstations to determine, and the test frequency is $0.1\text{-}10^5$Hz, and the alternating polarization is 5mV.

2.2.3 Research methods of tensile strength

Tensile strength of polymer diaphragms was measured by XLW cell diaphragm tensile strength tester.

2.2.4 Research methods of electrochemical stability window

Electrochemical stability window can be used to characterize the electrochemical stability of the battery system. The blocking type battery (SS/electrolyte/SS) was equipped in the vacuum glove box. The linear scanning measurement was carried out with the American type 2273 electrochemical workstations to study the change of the current density with the voltage. The polymer diaphragm is sandwiched between the stainless steel sheet and the lithium wafer to form a Li/PE/SS measuring system. The stainless steel sheet is used as the working electrode and lithium tablets as a pair of electrodes. The scanning potential range is 3-5.5V, and the scan rate is 5mV/s.

2.2.5 Charging and discharging test

In this paper, the performance of lithium-ion batteries using porous organic separators is measured by constant current charge and discharge in a specified voltage range. The charging test is to connect the battery of the external power supply and charge it by constant current or constant pressure. The electrical energy of the outer circuit is converted into chemical energy stored in the battery, while recording the voltage or current of the battery in the process changes from time. The discharge test is to connect the battery of the load. When the chemical energy in the batteries are converted to electrical energy and the load is supplied, the operating voltage of the battery is recorded over time. The result of charge and discharge to test is an important criterion to judge the performance of the battery. The battery life, charge to discharge efficiency, capacity and other electrochemical properties can be read out from the test results of charge and discharge test.

This experiment adopts the TC-5X high precision detection system of Shenzhen new Weier Electronics company Limited to test charge and discharge performance. The test conditions are as follows: charge and discharge rate is 0.1C; voltage range is 2.5~4.4V; test temperature is room temperature. The charge and discharge performance of the separator material was characterized by the electrochemical performance test.

2.2.6 SEM research methods

The micro-morphology of polymer diaphragm was analyzed by using S-3400N scanning electron microscope of Japan Hitachi Corporation. The surface morphology of the polymer diaphragm was observed by SEM, and the surface structure was observed by surface topography characterization. The surface structure of the polymer diaphragm also has a great influence on the comprehensive performance of the separator, especially on the stability of the electrode interface. The smoother the surface is, the better the stability of the interface is.

2.2.7 Research methods of infrared spectroscopy

The surface total reflection spectrum of the polymer diaphragm was measured, the test range was $600 \sim 2000 cm^{-1}$, and the resolution was $2 cm^{-1}$. According to the chemical bonds and groups in the different molecular structure, the infrared absorption spectrum frequency will change regularly, so as to determine the composition and structure information of polymer.

2.2.8 XRD research methods

Using X-ray diffraction analysis to determine the crystallinity of polymer diaphragm, the crystallinity can affect the ion conduction capacity and conduction mode. The specific method is: the scanning speed is $2°/min$ in the range of $5°-70°$; the radiation source is Cu-Kα; tube current is 40Ma; voltage is 40KV.

3. RESULTS AND DISCUSSION

3.1 Orthogonal experimental data analysis

Orthogonal experimental data processing is shown in Table 3, 4.

Table 3. Orthogonal experimental data analysis I

experiment	A	B	C	D	E	Porosity /%	Conductivity /mS·cm^{-1}
1	1	1	1	1	1	66.93	2.083
2	1	2	2	2	2	71.18	2.209
3	1	3	3	3	3	67.45	2.089
4	1	4	4	4	4	73.58	2.088
5	2	1	2	3	4	70.93	2.133
6	2	2	1	4	3	78.45	2.370
7	2	3	4	1	2	72.09	2.026
8	2	4	3	2	1	55.09	1.431
9	3	1	3	4	2	88.82	3.298
10	3	2	4	3	1	79.62	2.924

11	3	3	1	2	4	81.18	3.031
12	3	4	2	1	3	92.89	3.692
13	4	1	4	2	3	57.42	1.968
14	4	2	3	1	4	81.31	2.863
15	4	3	2	4	1	70.98	2.574
16	4	4	1	3	2	67.38	2.385

Table 4. Orthogonal experimental data analysis II

Level	A	B	C	D	E
Porosity	69.79	71.03	73.49	78.31	68.16
	69.14	77.64	76.49	66.22	74.87
	85.63	72.93	73.17	71.35	74.05
	69.27	72.24	70.68	77.96	74.17
Range R	16.49	6.61	5.81	12.09	6.71
Order of factors			DAEBC		
Optimal scheme			A3B2C2D1E2		

Level	A	B	C	D	E
conductivity	2.117	2.371	2.467	2.666	2.253
	1.990	2.592	2.652	2.160	2.480
	3.236	2.430	2.420	2.383	2.530
	2.448	2.399	2.252	2.583	2.529
Range R	1.246	0.221	0.400	0.506	0.276
Order of factors			ADCEB		
Optimal scheme			A3B2C2D1E3		

By analyzing the experimental data, it is concluded that the addition of nano-TiO_2 has a certain effect on increasing the porosity and ionic conductivity. TiO_2 is uniformly dispersed in the system, making the strength of the diaphragm significantly better than that of the diaphragm without adding nano-TiO_2. However, the content of nano-TiO_2 in this orthogonal experimental design is not a major factor of the selected indicators. In order to analyze the optimal ratio of every factor of the experiment, we will now conduct a single factor experiment for analysis.

3.2 Porosity

A single factor experiment was used to test the effect of TiO_2 addition on the porosity of the diaphragm .
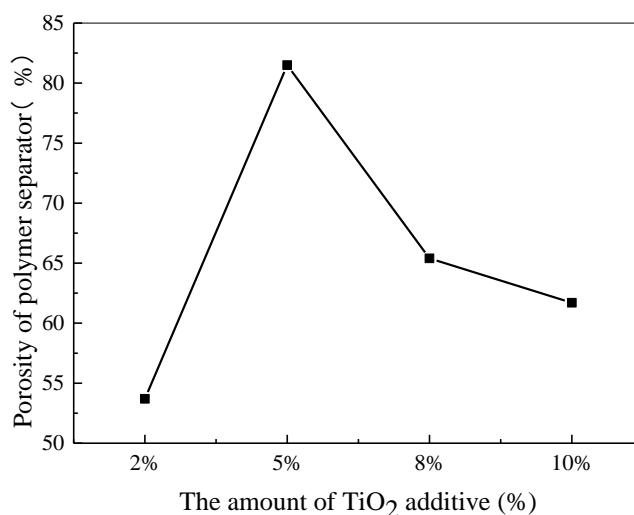
Figure 2. Porosity variations of polymer separators with different content of TiO$_2$ additive.

The comparison of the porosity of different TiO$_2$ is shown in Fig 2. It can be seen from Fig 2 that the porosity presents the first rising and then lower trend with the increase in TiO$_2$ content. With the increase in nano-TiO$_2$ content of 2% to 5%, inorganic nanoparticles dispersed evenly on the polymer diaphragm surface, reducing the pore collapse to keep the structure relatively intact. This situation is similar to the results reported previously [27], the PVDF separators with grafted polymers exhibited the better pore distribution.When the TiO$_2$ content is 5%, the porosity reaches a maximum of 81.5%. However, as the content of nano-TiO$_2$ increases, the porosity gradually decreases. It has been reported [28] that the decrease in porosity is caused by the large accumulation of nano-TiO$_2$ on the surface of the membrane to block the pores. In addition, the maximum porosity of the PVDF/PMMA/PEG separators studied by Gao [23] were 70.3%, and the maximum porosity of the PVDF/PMMA/HFP separators studied by Li [29] were 77.9%. It can be concluded that the PVDF separators are modified by the appropriate amount of nano-TiO$_2$, can make the separators pores intact relatively and rich, and can improve the porosity of the separators. This is also one of the reasons why the ionic conductivity of the diaphragm after the modification of TiO$_2$ has been improved.

3.3 Ionic conductivity

The single factor experiment was used to test the effect of TiO$_2$ addition on the ionic conductivity of the diaphragm.

The test results of ionic conductivity with different TiO$_2$ additions are shown in Figure 3.
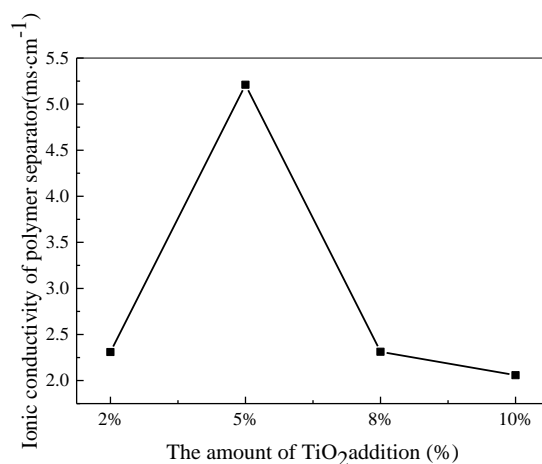
Figure 3. Ionic conductivity variations of polymer separators with different content of TiO$_2$ additives.

The nano-TiO$_2$ particles are introduced into the polymer electrolyte. Since the dielectric constant of the nano-particles is high, it can promote the dissociation of the lithium salt, thereby increasing the carrier concentration. Miao et al [30, 31]. showed that the addition of TiO$_2$ to the polymer separators helps to reduce the degree of crystallinity, increase mechanical strength, and promote the transport of Li$^+$ at the filler particles boundaries. In addition, the Ti atom can interact with the ester functional group to reduce the crystallinity, increase the proportion of amorphous regions, facilitate the rapid migration of lithium ions, and thus can increase the room temperature ionic conductivity. However, the amount of nano TiO$_2$ is not the more the better, too much nano TiO$_2$ will clog the channel, which is not conducive to lithium ion migration. According to Fig 3. It can be seen that with the increase in nano-TiO$_2$ content, the ionic conductivity increases firstly and then decreases, and reaching the maximum value of 5.2mS/cm when the content of TiO$_2$ is 5%. Other than this, The LiFePO$_4$/PVDF-GFM/Li types separator, which was studied by in-situ polymerization by Liang [32], has an ionic conductivity of 1.13 mS/cm. and the maximum ionic conductivity of the PVDF/PMMA/HFP separators studied by Li [29] was 1.57 mS/cm. By comparison, it can be found that the PVDF/PMMA/PEG/TiO$_2$ type diaphragm has excellent ionic conductivity and has great improvement in the performance of lithium ion battery.

3.4 Tensile strength

According to the GB/T1040.3-2006 Plastic Tensile Testing, ASTM D882-09 Standard Test Method of Tensile Properties of Thin Plastic Sheeting determination of polymer separator tensile strength 115.9MPa, The tensile strength of PVDF/LiPVAOB GPE membrane researched by Liang is 32.4 MPa [32]. Studies have shown that this increase in tensile strength is due to the interaction between the ester groups of PMMA and the hydroxyl group of TiO$_2$ [33], and the α-methyl groups of PMMA can be substituted for Ti element. So it can be concluded that the separator after modification by TiO$_2$ has excellent mechanical properties, which can avoid the shrinkage of the separator and

pevent the occurrence of contact short-circuit between positive and negative terminals of lithium ion battery. It meets the performance requirements of lithium ion battery separators.

3.5 Electrochemical stability window
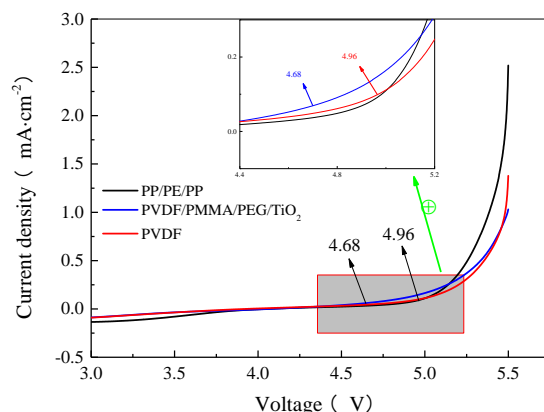
Figure 4. Linear sweep voltammetry curves of PP/PE/PP type (black line), PVDF/PMMA/PEG/TiO$_2$ type (blue line) and PVDF type (red line) of polymer separator.

Electrochemical stability is an important index of polymer diaphragm. Fig. 4 is a LSV curve obtained by the 5mv scanning speed in the 3~5.5V voltage range of the three different polymer separators. From the linear sweep voltammetry, it can be seen that the polymer diaphragm is relatively stable at a small voltage at the beginning of the scan. However, as the scan potential increases, the current rises sharply when the potential reaches a certain level. It showed that the polymer diaphragm produces electrochemical reactions and begins to decompose. The electric potential is the electrochemical stability window of the polymer separator [23].

From Fig 4, the decomposition voltage of the PVDF/PMMA/PEG/TiO$_2$ types polymer diaphragm was 4.68V. This result was similar to previous research reported [27], and the PVDF-LiPVAOB GPE diaphragm studied by Liang has an electrochemical stability of 4.8V [32]. Other than this, the decomposition voltage of the PVDF/HFP/SiO$_2$ type polymer separator studied by Aravindan [34] was 4.7V. It can be seen that the decomposition voltage of the PVDF/PMMA/PEG/TiO$_2$ types polymer diaphragm is lower slightly than others, but it still can meet the charging voltage safety requirement of the lithium-ion batteries. Analysis has led to the conclusion that it is due to the effect of Ti atoms and ester functional groups on the addition of TiO$_2$, which results in a decrease in the crystallinity of the system. The proportion of amorphous regions increases. The oxygen atoms compete with the oxygen atoms on the segments of lithium ions, weakening the bonds between the atoms on the segments and the lithium ions, leading to electrolyte decomposition voltage decreased.

3.6 Charging and discharging analysis

Fig 5 is the first charge and discharge curve of the modified polymer diaphragm. The durable rate performance of lithium-ion battery capacity is an important feature of practical application [35]. It can be seen from the figure, the first charge using a polymer separator battery capacity is

149.375mAh/g, the initial discharges capacity is 128.535 mAh/g, and the first coulomb efficiency was 86.05%. In contrast, the commercial separator battery has a capacity of about 120 mAh/g. After repeated cycles, the reversible capacity of the commercial diaphragm decreased dramatically. It is attributed to three main reasons, including the loss of cathode active materials, the leakage of active electrolyte and the irreversible production of new solid electrolyte interphase (SEI) [27, 36-38] In the PF/AL-PE separator studied by Dan Li, the PF/AL-PE separator showed improved cycle performance at room temperature compared to the original PE separator. The PF/AL-PE separator has a high discharge capacity of more than 130 mAh/g [39]. In the Al_2O_3/PEO separator studied by Park [40], the initial charge and discharge capacity is around 75.3 mAh/g. It is known from the above comparison that the blend modified PVDF separator meets the performance of the battery separator, which is greater than the efficiency of the unmodified PVDF separator. As described in the previous section, its superior performance is attributed to the high porosity and the high ionic conductivity.
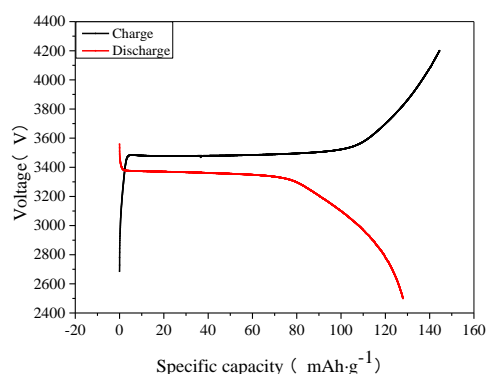
Figure 5. First charge and discharge curve of modified PVDF/PMMA/PEG/TiO_2 type of polymer separator.

3.7. SEM analysis
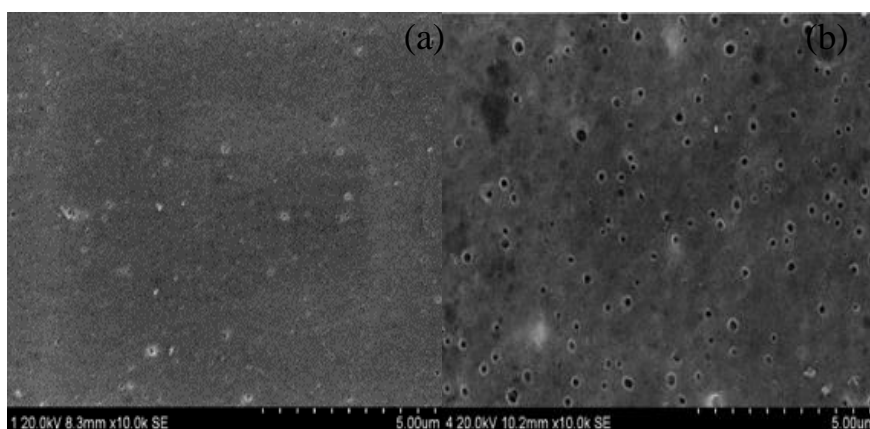
Figure 6. SEM image of commercial diaphragm and porous diaphragm. (a): commercial diaphragm after amplifying 10,000 times, (b): modified polymer separator after amplifying 10,000 times.

Fig 6 is a comparison chart of the scanning electron microscope of the lithium ion battery commercial diaphragm and the PVDF/PMMA/PEG/TiO$_2$ type polymer separator doped with 5% nano-TiO$_2$. Obviously, it is consistent with the reported [27] that dense pores were distributed over the polymer membrane, which could store the liquid electrolyte and provide sufficient channels for ion conduction. From the Fig 6, it can be seen that the two diaphragm surfaces are more homogeneous. The lithium ion battery commercial diaphragm's pores are few and the pores are smaller. It is not easy to see the pore information on figure (a) of amplifying 10,000 times. On the contrary, after amplifying 10000 times, it can be clearly seen that there are many pores presents from the figure (b) and these pores structures are rich and uniform. It is precisely because of this diaphragm structure, which has a larger aperture than the commercial diaphragm. So that it provides a channel for lithium ion migration, gives it a good ionic conductivity. These observations also confirmed the results of the previous study on diaphragm performance [28].

3.8 Infrared spectrum analysis

Fig 7 is a comparison of the infrared spectra of the PVDF diaphragm and the PVDF/PMMA/PEG/TiO$_2$ polymer diaphragm. By comparison, it can be seen that the same wave peaks are 1400cm^{-1}, which is the deformation rocking vibration of CH$_2$. The position 1200 cm^{-1} and 870 cm^{-1} are vibration peaks of C-C skeleton. These observations also confirmed previous studies [41]. The bands of 840 cm^{-1} and 973 cm^{-1} correspond to β- and α- phase PVDF crystals. Moreover, the bands of 1170 cm^{-1} is the CF$_2$ stretching vibration peaks. The bands of 1066cm^{-1} and 794 cm^{-1} are the vibrational absorption peaks of crystalline phase. The difference is that the absorption peaks corresponding to the red curve, in which the bands of 1600 cm^{-1} and 760 cm^{-1} correspond to Characteristic peaks of TiO$_2$. In addition, compared to the corresponding position (blue line), it can be found that the PVDF crystal peaks (red line) intensities in the 840 and 973 bands are decreased. This is due to the interaction between the hydroxyl group of TiO$_2$ and the ester functional group that cause decrease in crystallinity. This in turn confirms that the polymeric diaphragm (subsection 3.3) has excellent ionic conductivity. And also the bands of 1729cm^{-1} are the stretching vibration peak of C=O in Poly-Methyl-Methacrylate, the bands of 1149cm^{-1} are the absorption peak of C-O in polyethylene glycol. From the above results, it can be concluded that the prepared materials contain Poly-Methyl-Methacrylate (PMMA) and polyethylene glycol (PEG), and nano-TiO$_2$ is well dispersed in the polymer separator.
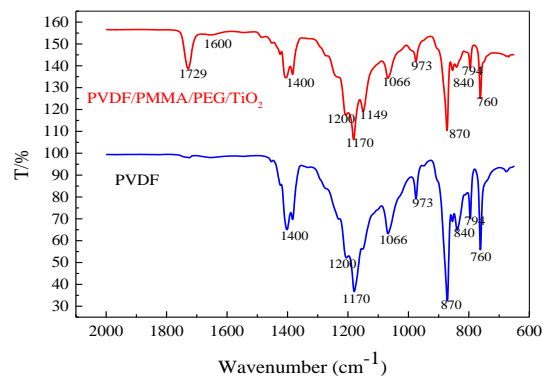
Figure 7. Infrared spectra curves of PVDF/PMMA/PEG/TiO$_2$ type (red line) and PVDF type (blue line) of polymer separator.

3.9 XRD analysis

Fig 8 is a XRD contrast diagram of PVDF diaphragm and PVDF/PMMA/PEG/TiO$_2$ type polymer diaphragm.

As shown in Fig 8, The PVDF has three diffraction peaks of 17, 20 and 27. It has been reported [42] that after the addition of HTPB-g-MPEG, the diffraction peaks at 17 and 20 were wider, and the bread peaks were more obvious, indicating the more amorphous state. Compared with the PVDF based separator, the diffraction peaks of PVDF/PMMA/PEG/TiO$_2$ polymer separator disappeared at 2θ angle of 17° and 39°, indicating that the crystallinity of the PVDF/PMMA/PEG/TiO$_2$ polymer diaphragm was lower, which meet the above research result. But the diffraction peaks not only did not disappear at 2θ angles at 20° and 27° but also increase. It was analyzed that this was caused by doped nano-TiO$_2$. The intensity of the TiO$_2$ characteristic diffraction peaks at 20° and 27° were enhanced to cancel the attenuation of the PVDF diffraction peaks. The characteristic diffraction peaks of the two types nano-TiO$_2$ were shown by the green and blue lines in Figure 8, and the upper left and upper right are the two types TiO$_2$ card information, and the diffraction peaks of 2θ angles at 36° and 54° are also the diffraction peaks of TiO$_2$. In addition, the PVDF/HFP type diaphragms were studied by Aravindan [34], after adding nano-SiO$_2$ or Al$_2$O$_3$, the diffraction peaks intensity of 2θ angles at 17° and 39° were decreased. These results indicate that the nano-TiO$_2$ particles have been introduced into the polymer separators, and can reduce the crystallinity effectively of the polymer separators and increase the ionic conductivity of the separators.
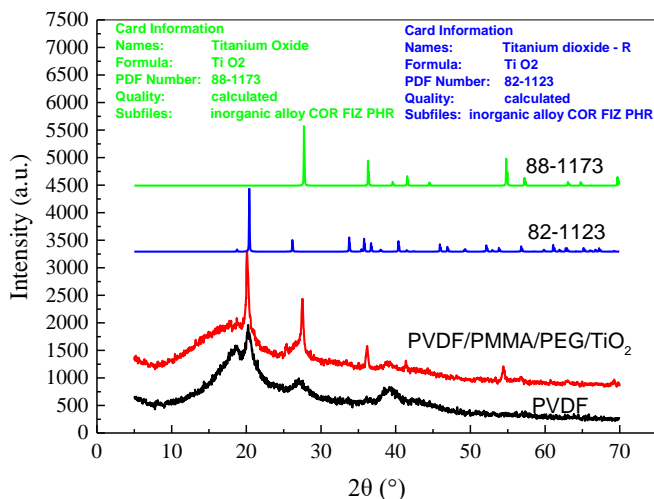
Figure 8. XRD patterns of Titanium Oxide (green line), Titanium dioxide–R (blue line) and PVDF/PMMA/PEG/TiO$_2$ type (red line), and PVDF type (black line) of polymer separator.

4. CONCLUSION

The method of preparing a separator by mixing PMMA and adding inorganic nano-TiO$_2$ has a significant influence on the ionic conductivity of the separator. With the addition of TiO$_2$, the ionic conductivity increases first and then decreases. When the addition amount of TiO$_2$ is 5%, the separator has the best performance, and the ionic conductivity increases from 2.848 mS/cm to 5.2 mS/cm.

Compared with the commercial separators, after the addition of inorganic nano TiO$_2$, the crystallinity of the polymer diaphragm is effectively reduced because of the high surface area and high dielectric constant of TiO$_2$, and thus the polymer membrane has a high ionic conductivity. Moreover, the surface of the polymer separator sheet is very uniform and the pore structure is complete and rich.

In addition, the PVDF separator modified by TiO$_2$ had a charging capacity of 149.375 mAh/g, a discharge capacity of 128.535 mAh/g, and a coulomb efficiency of 86% in the charge-discharge cycle test of the battery. The results show that the performance of the PVDF separator modified by TiO$_2$ has been greatly improved and can replace the commercial diaphragm.

References

1. P. Arora, Z. J. Zhang, *Cheminform*, 35 (2004) 4419-4462.
2. M. Xiong, H. l. Tang, M. Pan, *Carbohydrate Polymers*, 101 (2014) 1140-1146.
3. L. T. Hong, L. Wang, H. M. Ye, J. J. Yi, *Polymer Bulletin*, 6 (2017) 59-67.
4. D. Li, D. Qin, F. Nie, *J. Mater. Sci. Technol*, 5 (2018) 1-12.
5. Y. Zhang, Z. Wang, H. Xiang, *J. Membrane. Sci.*, 509(2016) 19-26.
6. S. Ramesh, R. Shanti, R. Durairaj, *J. Non-Cryst. Solids,* 357 (2011) 1357-1363.
7. S. Sekhon, H. P. Singh, *Solid State Ionics,* 152 (2002) 169-174.
8. S. Ramesh, O. P. Ling, *Polymer Chemistry*, 5 (2010) 702-707.
9. B. Li, Y. Li, D. Dai, K. Chang, *Acs. Appl. Mater. Inter*, 34 (2015) 20184-20189.

10. Q. Shi, M. Yu, X. Zhou, *J. Power Sources*, 103 (2002) 286-292.
11. Q. Xiao, X. Wang, W. Li, *J. Separator. Sci.*, 334 (2009) 117-122
12. Z. H. Li, C. Cheng, X. Y. Zhan, *Electrochim Acta*, 54 (2009) 4403-4407.
13. Z. H. Li, P. Zhang, H. P. Zhang, *Electrochem. Commun,* 10 (2008) 791-794.
14. J. D. Jeon, S. Y. Kwak, *J. Separator. Sci.,* 286 (2006) 15-21.
15. J. Fang, A. Kelarakis, Y. W. Lin, C. Y. Kang, Phys. Chem. Chem. Phys, 13 (2011) 14457-14461.
16. Q. Shi, M. Yu, X. Zhou, *J. Power Sources*, 103 (2002) 286-292.
17. Q. Xiao, X. Wang, W. Li, *J. Separator. Sci.,* 334 (2009) 117-122.
18. Z. H. Li, C. Cheng, X. Y. Zhan, *Electrochim Acta*, 54 (2009) 4403-4407.
19. Z. H. Li, P. Zhang, H. P. Zhang, *Electrochem. Commun,* 10 (2008) 791-794.
20. J. D. Jeon, S. Y. Kwak, *J. Separator. Sci.,* 286 (2006) 15-21.
21. G. LoebS, S. Sourirajian, *Adv. Chem. Ser*, 38 (1963) 117-132.
22. Y. Lu, H. Chen, L. I. Bo, *J. Functional Polymers*, 15 (2002) 171-176.
23. H. Gao, A. Y. Chen, S. B. Wang, *Funct. Mater. Lett,* 46 (2015) 15138-15141.
24. A. K. Solarajan, V. Murugadoss, *Nano Hybrids & Composites*, 14 (2017) 1-15.
25. J. Cao, L. Wang, M. Fang, *J. Power Sources,* 246 (2014) 499-504.
26. H. F. Xiang, J. J. Chen, *J. Power Sources*, 196 (2011) 8651-8655.
27. M. K. Guo, B. H. Zhou, J. Hu, J. R. Wang, D. He, X. L. Xie, *J. Membrane. Sci.,* 564 (2018) 663-371.
28. J. Zhang, C. Ma, Q. Xia, J. Liu, Z. Ding, M. Xu, *J. Membrane. Sci.*, 497 (2016) 259-269.
29. X. F. Li, D. Z. Wu, *J. Separator. Sci.,* 45 (2014) 368-374.
30. R. Miao, B. Liu, Z. Zhu, Y. Liu, J. Li, X. Wang, *J. Power Sources*, 184(2008) 420-426.
31. C. M. Costa, M. M. Silva, *RSC Advances*, 3 (2013) 11404.
32. S. S. Liang, W. Q. Yan, X. Wu, *Solid State Ionics*, 318 (2018) 2–18.
33. J. D. Jeon, M. J. Kim, S. Y. Kwak, *J. Power Sources,* 162 (2006) 1304-1311.
34. V. Aravindan, P. Vickraman, *J. Appl. Polym. Sci.,* 10 (2008) 1314-1322.
35. J. Hao, G. Lei, Z. Li, L. Wu, Q. Xiao, L. Wang, *J. Membrane Sci.*, 428 (2013)11-16.
36. J. Xu, R. D. Deshpande, J. Pan, Y. T. Cheng, V. S. Battaglia, *J. Electrochem. Soc.* 162 (2015) A2026-A2035.
37. M. Dubarry, B. Y. Liaw, *J. Power Sources* 194 (2009) 541-549.
38. K. L. Gering, *Electrochim. Acta,* 228 (2017) 636-651.
39. D. Li, D. Qin, F. Nie, *J. Mater. Sci., 24* (2018) 1-12.
40. K. Park, J. H. Cho, *J. Power Sources*, 263 (2014) 52-58.
41. J. Zhang, Z. Wang, X. Zhang, X. Zheng, Z. Wu, *Appl. Surf. Sci.,* 345 (2015) 418-427.
42. H. Li, D. H. Niu, H. Zhou, C. Y. Chao, L. J. Wu, *Appl. Surf. Sci.*, 440 (2018) 186-192.